Nonlinear stability of oscillatory wave fronts in chains of coupled oscillators

A. Carpio*
Departamento de Matemática Aplicada, Universidad Complutense de Madrid, 28040 Madrid, Spain
(Received 6 October 2003; published 12 April 2004)

We present a stability theory for kink propagation in chains of coupled oscillators and a different algorithm for the numerical study of kink dynamics. The numerical solutions are computed using an equivalent integral equation instead of a system of differential equations. This avoids uncertainty about the impact of artificial boundary conditions and discretization in time. Stability results also follow from the integral version. Stable kinks have a monotone leading edge and move with a velocity larger than a critical value which depends on the damping strength.

DOI: 10.1103/PhysRevE.69.046601 PACS number(s): 45.05.+x, 83.60.Uv, 05.45.−a

I. INTRODUCTION

The dynamics of waves in chains of coupled oscillators is the key to understanding the motion of defects in many physical and biological problems: motion of dislocations [1,2] or cracks [3] in crystalline materials, atoms adsorbed on a periodic substrate [4], motion of electric field domains and domain walls in semiconductor superlattices [5], pulse propagation through myelinated nerves [6] or cardiac cells [7] and so on. A peculiar feature of these spatially discrete systems is that wave fronts and pulses get pinned for entire intervals of a control parameter such as an external force. Typically, wave fronts do not move unless the external force surpasses a control value. Such is the case with the static and dynamic Peierls stresses in dislocation dynamics [2,8] or the dynamic and static friction coefficients [9] in continuum mechanics. Pinning and motion of wave fronts also explain the relocation of static electric field domains and the self-oscillations of the current in semiconductor superlattices [5].

Wave front motion in systems of nonlinear oscillators modeling these phenomena are easier to analyze in the overdamped case, and less so if inertia is important. In the presence of inertia, the wrong choice of boundary conditions or the numerical method may suppress important solutions of the original system or yield spurious oscillations. Thus two problems that are important in all spatially discrete systems acquire even more importance: how do we find wave fronts and what are their stability properties?

We have solved the first problem in a recent work [10] by choosing a damped system of oscillators with a piecewise linear source term, see also Refs. [3,11,12]. Our results show explicitly the existence of kinks with oscillatory profiles for systems with little or no damping. In the latter case, these wave fronts have at least one tail with nondecaying oscillations that extend to infinity. Depending on the control parameter, branches of oscillatory wave fronts may exist, coexisting for entire intervals of the external force and even coexisting with pinned wave front solutions. These facts, long-lived oscillatory profiles and coexistence of wave front branches, highlight the importance of ascertaining the stability properties of these solutions. This is not easy and not many results are known.

To be precise, let us consider oscillator chain:

$$mu_n''+\alpha u_n'=K(u_{n+1}-2u_n+u_{n-1})-V'(u_n)+W. \quad (1)$$

We nondimensionalize the model by choosing the time scale $\sqrt{ma^2/v_m}$, where a is the interatomic distance, m is the mass, and v_m the strength of the on-site potential. For a piecewise parabolic potential, the nondimensional equation is

$$u_n''+\gamma u_n'=D(u_{n+1}-2u_n+u_{n-1})-g(u_n)+F, \quad (2)$$

$$g(s)=\begin{cases} s, & s<\frac{1}{2} \\ s-1, & s\geq\frac{1}{2}. \end{cases} \quad (3)$$

Here γ and D are the ratios between friction and inertial forces, and between the strengths of the harmonic and on-site potentials, respectively. $F=Wa/v_m$. Atkinson and Cabrera [11] conjectured that only two branches of kinks are stable for Eqs. (2)–(3).

(1) A branch of static kinks for values of the control parameter $|F|$ below a static threshold $F_{cs}(D)$.

(2) A branch of traveling kinks for $|F|$ above a dynamic threshold $F_{cd}(\gamma,D)\leq F_{cs}(D)$, with speeds c larger than a minimum speed $c_{cd}(\gamma,D)$. This family has a distinctive feature compared to eventual slower waves [10]. The leading edge of the kink is monotone whereas the trailing edge may develop oscillations.

The values F_{cs} and F_{cd} correspond to the static and dynamic Peierls stresses of the literature on dislocations [2]. In the overdamped limit $\gamma\to\infty$, $F_{cs}=F_{cd}$ and stable wave fronts can be found with arbitrarily small speeds [13].

In a previous paper [10], we checked numerically the validity of Atkinson and Cabrera's conjecture. This is a delicate affair and further analytical work is clearly desirable. In fact, most numerical studies of kink propagation truncate the infinite chain to a finite chain, fix some boundary conditions, and then use a Runge-Kutta solver (or variants) to investigate the dynamics of kinklike initial configurations. For instance,

*Email address: ana_carpio@mat.ucm.es

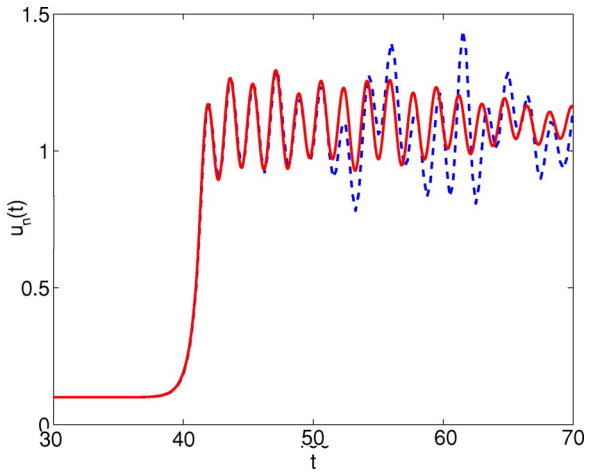

FIG. 1. (Color online) Trajectory $u_n(t)$ computed by solving a truncated system of differential equations (dashed) and by integral expressions (solid) for $\gamma=0.02$, $D=4$, $F=0.1$, $n=-70$.

Peyrard and Kruskal [14] applied this procedure to study kinks in the conservative Frenkel-Kontorova model, including friction near the ends of the truncated chain in an attempt to avoid reflections. On the other hand, our analytical work [10] shows that traveling kinks oscillate with almost uniform amplitude even for small damping. Then, artificial boundary conditions and time discretization may greatly distort their shape and dynamics. In fact, using Runge-Kutta methods to solve Eq. (2) with constant boundary conditions generates reflections at the boundary, as shown in Fig. 1, after a waiting time depending on the size of the lattice. Such oscillations end up distorting the right tail and may completely alter the shape of the kink giving rise to a complex oscillatory pattern.

A good way to avoid the spurious effects of inappropriate boundary conditions is to recast Eq. (2) as an integral equation. Integral reformulations provide an analytical expression for the solutions of Eq. (2) which we use to develop numerical algorithms. Spurious pinning and spurious oscillations are suppressed. The introduction of these numerical methods based on integral reformulations of Eq. (2) is one of our main results.

The main analytical results of this paper concern the nonlinear stability of stationary and traveling wave fronts in chains of oscillators. Besides leading to good numerical methods, we have also used the integral equation formulation to investigate the nonlinear stability of wave front patterns. We provide a criterion to decide whether certain kinklike initial configurations evolve into stable wave front patterns. In discrete overdamped models the nonlinear stability of traveling wave fronts follows from comparison principles. This strategy was applied to the study of domain walls in discrete drift-diffusion models for semiconductor superlattices in Ref. [15].

Common belief is that comparison principles do not hold in models with inertia. This belief is wrong. How can we assess the stability of traveling wave fronts in such models? For large damping, we can directly compare solutions of Eq. (2) using its equivalent formulation as an integral equation thanks to the positivity of the Green functions. As the damping decreases, we can ignore the oscillatory tails of the fronts and compare the monotone leading edges of the solutions, which drive their motion. The process of comparing solutions is technically more complex than in the overdamped case because the Green functions change sign, and the fronts have oscillatory wakes. Summarizing, there are two key ingredients for stability. First, the leading edges of the fronts have to be monotone. Second, the Green functions of the linear problem must be positive for an initial time interval, of duration comparable to the time the front needs to advance one position. This restricts the possible values of the propagation speed for small damping: only fast kinks are shown to be stable. Our methods are quite general and can be extended to Frenkel-Kontorova models with smooth sources [16] at the cost of technical complications.

The paper is organized as follows. In Sec. II we introduce a numerical algorithm and discuss the stability of static kinks. The stability theory for traveling kinks is presented in Sec. III. In Sec. IV we discuss the role of oscillating Green functions in the appearance of static and dynamic thresholds due to coexistence of stable static and traveling waves. In Sec. V we briefly comment on extensions to oscillator chains with smooth cubic sources. Section VI contains our conclusions. Basic details on the pertinent Green functions are recalled in Appendixes A and B. Proofs of our main stability results can be found in Appendixes C and D.

II. STATIC KINKS

The stationary wave fronts s_n for Eq. (2) increase from $s_{-\infty}=F$ to $s_\infty=1+F$ and solve the second-order difference equation

$$D(s_{n+1}-2s_n+s_{n-1})-s_n+H(s_n-\tfrac{1}{2})+F=0 \qquad (4)$$

in which $H(x)$ is the Heaviside unit step function. These fronts are translation invariant. We fix their position by setting $s_0<\frac{1}{2}<s_1$. Then, $s_n=F+ar^n$ for $n\leqslant 0$ and $s_n=1+F-br^{-n}$ for $n\geqslant 1$, where $r=(2D+1+\sqrt{4D+1})/2D$. Inserting these formulas in Eq. (4) for $n=0$ and $n=1$, we find a and b. Our construction of the stationary fronts s_n is consistent with the restriction $s_0<\frac{1}{2}<s_1$ when $|F|\leqslant F_{cs}(D)$. Figure 2(a) shows a static wave front for $D=4$ and $F=0.05$. As D grows, the number of points in the transition layer between the constants increases.

A. Stability

A stationary wave front s_n is stable for the dynamics (2) when chains initially close to s_n remain near s_n for all $t>0$, as shown in Fig. 2. The initial states chosen in this figure are $u_n^0=F+\delta_n^0$ when $n\leqslant 0$, $u_n^0=1+F+\delta_n$ when $n\geqslant 1$ and $u_n^1=\delta_n^1$. Both δ_n^1 and δ_n^0 are small random perturbations.

To find the stable profiles, we proceed as follows. Let u_n^0 and u_n^1 be the initial position and velocity of the chain. In terms of Green functions calculated in Appendix A, $u_n(t)$ is given by Eq. (A12) with $f_k(t)=F+H(u_k(t)-\frac{1}{2})$:

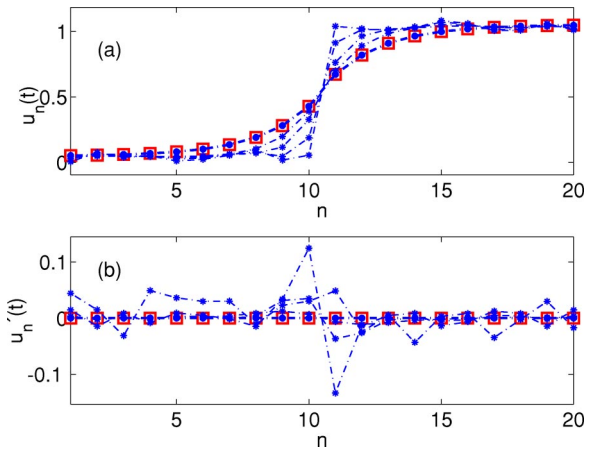

FIG. 2. (Color online) Convergence to a static kink s_n when $D=4$, $\gamma=10$, and $F=0.05$: (a) asterisks $u_n(t)$, squares s_n, (b) asterisks $u_n'(t)$, squares $s_n'=0$.

$$u_n(t)=\sum_k G_{nk}^0(t)u_k^1+\sum_k G_{nk}^1(t)u_k^0 + \int_0^t \sum_k G_{nk}^0(t-z)H\left(u_k(z)-\frac{1}{2}\right)dz + F\int_0^t \sum_k G_{nk}^0(t-z)dz. \tag{5}$$

If initially $u_k^0<\frac{1}{2}$ for $k\leqslant 0$, $u_k^0>\frac{1}{2}$ for $k\geqslant 1$,

$$u_n(t)=\sum_k [G_{nk}^0(t)u_k^1+G_{nk}^1(t)u_k^0]+\int_0^t \sum_{k>0} G_{nk}^0(t-z)dz + F\int_0^t \sum_k G_{nk}^0(t-z)dz \tag{6}$$

as long as $u_k(t)<\frac{1}{2}$ when $k\leqslant 0$, $u_k(t)>\frac{1}{2}$ when $k\geqslant 1$. For $|F|<F_{cs}(D)$, the static wave front s_n with $s_0<\frac{1}{2}<s_1$ is a solution of Eq. (5) that satisfies

$$s_n=\sum_k G_{nk}^1(t)s_k+\int_0^t \sum_{k>0} G_{nk}^0(t-z)dz + F\int_0^t \sum_k G_{nk}^0(t-z)dz \tag{7}$$

for all $t>0$. Subtracting Eq. (7) from Eq. (6), we obtain:

$$u_n(t)-s_n=\sum_k [G_{nk}^0(t)u_k^1+G_{nk}^1(t)(u_k^0-s_k)]. \tag{8}$$

This expression holds for $t>0$ provided $u_n(t)-\frac{1}{2}$ does not change sign for any n and $t>0$. For which profiles $u_n(t)$ is this true? Let us select the initial state of the chain in the set:

$$\sum_{-\infty}^{\infty}|u_n^0-s_n|<M, \quad \sum_{-\infty}^{\infty}|u_n^1|<M, \quad M<R\min\left(1,\frac{1}{C_0+C_1}\right) \tag{9}$$

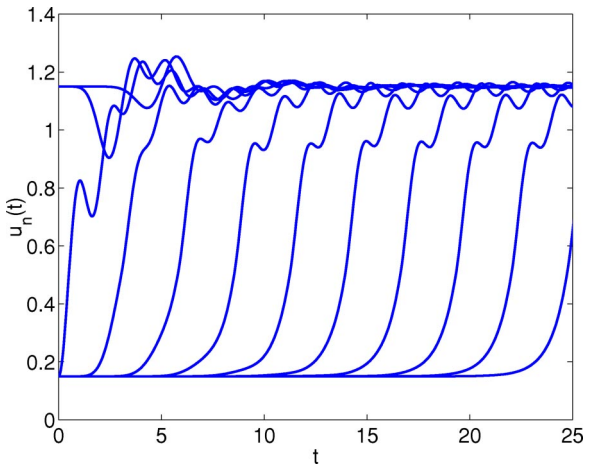

FIG. 3. (Color online) Trajectories $u_n(t)$, $n=8,4,0,-4,\ldots$ when $D=4$, $\gamma=0.4$, $F=0.15$.

with $R=\min(|s_0-\frac{1}{2}|,s_1-\frac{1}{2})$ and C_0,C_1 to be defined below. For $\gamma>0$, we show in Appendix B that $|G_{nk}^0|\leqslant C_0e^{-\eta t}$, $|G_{nk}^1|\leqslant C_1e^{-\eta t}$ with $\gamma>0$. This boundedness property of the Green functions and Eq. (9) yield

$$|u_n(t)-s_n|\leqslant (C_0+C_1)e^{-\eta t}M. \tag{10}$$

Then, $|u_n(t)-s_n|<R$ and $u_n(t)-\frac{1}{2}$ cannot change sign for any $t>0$. Moreover, $u_n(t)\to s_n$ as $t\to 0$.

In summary, the static kinks are exponentially and asymptotically stable in the damped case. Their basin of attraction includes all initial configurations u_n^0 and u_n^1 selected according to Eq. (9). In the conservative case, the static kinks are merely stable, but not asymptotically stable, because the previous argument with $\gamma=0$, $\eta=0$, $C_0=C_1=1$ only yields $|u_n(t)-s_n|\leqslant 2M$ for all times.

In the continuum limit $D\to\infty$, the number of points in the transition layer between constants increases and the distance between points decreases. Then, s_0 and s_1 tend to $\frac{1}{2}$ and the set of states (9) attracted by s_n shrinks as D grows. It becomes more likely that initial kinks in the chain propagate for a while and finally become pinned at some shifted static kink $v_n=s_{n+l}$, $v_{-l}<\frac{1}{2}<v_{-l+1}$.

B. Numerical algorithm

Formula (5) can be used to compute numerically the dynamics of the chain. However, the computational cost is high, due to the integral terms and the Green functions. In this section, we exploit the static front solutions s_n to reduce the cost and derive formulas for $u_n(t)$ which clarify the dynamics of the chain.

We will focus on initial kinklike initial states that generate ordered dynamics: $u_k(t)-\frac{1}{2}$ changes sign in an ordered way as the kink advances. Once the kink has passed, the configuration of the chain is close to a shifted static kink. That is why we use static kinks to obtain simplified expressions for $u_n(t)$. For instance, let us choose a piecewise constant initial profile $u_n^0=F$ for $n\leqslant 0$ and $u_n^1=1+F$ for $n\geqslant 1$, with $u_n^1=0$. For $F>0$, Fig. 3 shows that $u_{-k}(t)-\frac{1}{2}$ change sign at

time t_k, $k=0,1,\ldots$, with $t_0<t_1<\cdots<t_k<\cdots$. Eventually, the kink may get pinned at some static configuration and this process stops at some k. We then use a slightly modified version of the integral expression (7) for the static wave fronts to successively remove the integral terms in Eq. (5) and obtain simple formulas for $u_n(t)$ similar to Eq. (8). In this way, we find a relatively cheap algorithm for the computation of $u_n(t)$.

Let us describe the algorithm for $F\geqslant 0$ and an initial step-like state u_n^0 with $u_0^0<\frac{1}{2}<u_1^0$, as in Fig. 3. We must distinguish two cases: $0<F\leqslant F_{cs}(D)$ and $F>F_{cs}(D)$.

1. Case $0<F\leqslant F_{cs}(D)$

In this case, the stationary wave fronts can be used to generate a faster algorithm for obtaining $u_n(t)$. We remove the integrals in Eq. (5) by using the static wave front solution of Eq. (2), s_n, such that $s_0<\frac{1}{2}<s_1$.

Initial stage. Formula (8) allows to compute $u_n(t)$ up to the time t_0 at which $u_0(t)-\frac{1}{2}$ changes sign. For $t>t_0$ we compute $u_n(t)$ using as initial data $u_n(t_0)$ and $u_n'(t_0)$ at t_0. The latter is obtained differentiating Eq. (8):

$$u_n'(t_0)=\sum_k \left[\frac{dG_{nk}^0(t_0)}{dt}u_k^1+\frac{dG_{nk}^1(t_0)}{dt}(u_k^0-s_k)\right]. \quad (11)$$

For $t_0<t\leqslant t_1$, Eq. (5) becomes

$$u_n(t)=\sum_k [G_{nk}^0(t-t_0)u_k'(t_0)+G_{nk}^1(t-t_0)u_k(t_0)] + \int_{t_0}^t \sum_{k>-1} G_{nk}^0(t-z)dz+F\int_{t_0}^t \sum_k G_{nk}^0(t-z)dz. \quad (12)$$

Now, $u_{-1}(t_0)<\frac{1}{2}<u_0(t_0)$ and we must use the shifted stationary solution $v_n=s_{n+1}$, which satisfies $v_{-1}<\frac{1}{2}<v_0$. Observing that s_{n+1} solves Eq. (2) with initial data s_{n+1},0 at time t_0 we obtain the formula

$$s_{n+1}=\sum_k G_{nk}^1(t-t_0)s_{k+1}+F\int_{t_0}^t \sum_k G_{nk}^0(t-z)dz + \int_{t_0}^t \sum_{k>-1} G_{nk}^0(t-z)dz. \quad (13)$$

Subtracting Eq. (13) from Eq. (12) we find

$$u_n(t)=s_{n+1}+\sum_k G_{nk}^0(t-t_0)u_k'(t_0) + \sum_k G_{nk}^1(t-t_0)[u_k(t_0)-s_{k+1}], \quad (14)$$

up to the time t_1 at which $u_{-1}(t)-\frac{1}{2}$ changes sign.

Generic step. Once we have computed the time t_l at which $u_l(t)-\frac{1}{2}$ changes sign, we calculate the new initial data $u_n(t_l)$ and $u_n'(t_l)$:

$$u_n(t_l)=s_{n+l}+\sum_k G_{nk}^0(t_l-t_{l-1})u_k'(t_l) + \sum_k G_{nk}^1(t_l-t_{l-1})[u_k(t_l)-s_{k+l}], \quad (15)$$

$$u_n'(t_l)=\sum_k \frac{dG_{nk}^0}{dt}(t_l-t_{l-1})u_k'(t_l) + \sum_k \frac{dG_{nk}^1}{dt}(t_l-t_{l-1})[u_k(t_l)-s_{k+l}]. \quad (16)$$

Then the evolution of the chain for $t>t_l$ is given by the formula

$$u_n(t)=s_{n+l+1}+\sum_k G_{nk}^0(t-t_l)u_k'(t_l) + \sum_k G_{nk}^1(t-t_l)[u_k(t_l)-s_{k+l+1}], \quad (17)$$

until either $u_{-(l+1)}(t)-\frac{1}{2}$ or $u_{-l}(t)-\frac{1}{2}$ change sign. If $u_{-(l+1)}(t)-\frac{1}{2}$ changes its sign at a time t_{l+1}, we start a new step using s_{n+l+1} to compute $u_n(t)$. If $u_{-l}(t)-\frac{1}{2}$ reverses its sign at a time t_{l+1}, we start a new step using s_{n+l-1} to compute $u_n(t)$.

2. Case $F>F_{cs}(D)$

In this case, it is convenient to remove the integral in Eq. (5) by using as s_n the static wave front solution of Eq. (2) corresponding to an applied force $F=F_{cs}(D)$, and such that $s_0<\frac{1}{2}<s_1$. Recall that there are no stationary wave fronts for $F>F_{cs}$.

Initial stage. Subtracting Eq. (7) at $F_{cs}(D)$ from Eq. (6) we find

$$u_n(t)=s_n+\sum_k G_{nk}^0(t)u_k^1+\sum_k G_{nk}^1(t)(u_k^0-s_k) + (F-F_{cs})\int_0^t \sum_k G_{nk}^0(t-z)dz. \quad (18)$$

The remaining integral term can be removed by observing that 1 is a solution of Eq. (2) with $F=0$ and initial data $u_n(0)=1$, $u_n'(0)=0$:

$$1=\sum_k G_{nk}^1(t)+\int_0^t \sum_k G_{nk}^0(t-z)dz. \quad (19)$$

Multiplying Eq. (19) by $(F-F_{cs})$ and inserting the result in Eq. (18) we obtain

$$u_n(t)=s_n+(F-F_{cs})+\sum_k G_{nk}^0(t)u_k^1 + \sum_k G_{nk}^1(t)[u_k^0-s_k-(F-F_{cs})] \quad (20)$$

up to the time t_0 at which $u_0(t)-\frac{1}{2}$ changes sign. For $t>t_0$:

$$u_n(t)=s_{n+1}+(F-F_{cs})+\sum_k G^0_{nk}(t-t_0)u'_k(t_0)$$

$$+\sum_k G^1_{nk}(t-t_0)[u_k(t_0)-s_{k+1}-(F-F_{cs})],$$

$$u'_n(t_0)=\sum_k\left[\frac{dG^0_{nk}(t_0)}{dt}u^1_k+\frac{dG^1_{nk}(t_0)}{dt}(u^0_k-s_k-F+F_{cs})\right], \tag{21}$$

up to the time t_1 at which $u_{-1}(t)-\frac{1}{2}$ changes sign.

Generic step. Similar to the generic step for $F\leqslant F_{cs}$ but replacing s_n by $s_n+(F-F_{cs})$.

3. Numerical implementation

We will use Eqs. (17), (16), and (21) to study the dynamics of the chain in Sec. III. Due to translational invariance $G^0_{nk}=G^0_{n-k,0}$ and $G^1_{nk}=G^1_{n-k,0}$. To calculate $u_n(t)$, we only need to compute $G^0_{n0}(t)$, $G^1_{n0}(t)$ for a time interval $[0,T]$, $T\leqslant\max_l|t_{l+1}-t_l|$ and for $|n|\leqslant N$, where N is sufficiently large. We calculate the integrals $G^0_{n0}(t)$, $G^1_{n0}(t)$, $dG^0_{n0}(t)/dt$, and $dG^1_{n0}(t)/dt$ by means of the Simpson rule, choosing a step smaller than the period of the oscillatory factors. The value N is selected so as to make the error introduced by the truncated series $\Sigma_{|n-k|\leqslant N}$ sufficiently small. This is possible because the Green functions and their derivatives decay as $|n-k|$ grows.

A more general version of our algorithm will be presented elsewhere [16].

III. STABILITY OF TRAVELING KINKS

In this section we introduce a strategy to study the stability of traveling wave fronts in Eq. (2).

Traveling wave fronts are constructed by inserting $w_n(t)=w(n-ct)$ in Eq. (2) to produce a nonlinear eigenvalue problem for the profile $w(x)$ and the speed c. Assuming $w(x)<\frac{1}{2}$ for $x<0$ and $w(x)>\frac{1}{2}$ for $x>0$, the problem becomes linear. The wave profiles are computed as contour integrals, imposing $w(0)=\frac{1}{2}$ to find a relationship between c and F [11,10]. The law $F(c)$ and the shape of the wave profiles are controlled by the poles contributing to the contour integrals. The relevant poles depend on the strength of the damping. For large damping, we have complex poles with large imaginary parts. The dependence law $F(c)$ is monotonically increasing and the wave profiles are monotone. For small damping, poles with small imaginary parts become relevant, in increasing number as the speed c decreases. The function $F(c)$ oscillates for small speeds. Different oscillatory wave profiles with different speeds may coexist for the same F. At zero damping, those poles become real and the wave profiles develop nondecaying oscillations. For some ranges of speeds, the waves constructed in this way violate the restriction $w(x)<\frac{1}{2}$ for $x<0$ and $w(x)>\frac{1}{2}$ for $x>0$. Those ranges should be investigated with a modified technique allowing for a finite number of turning points.

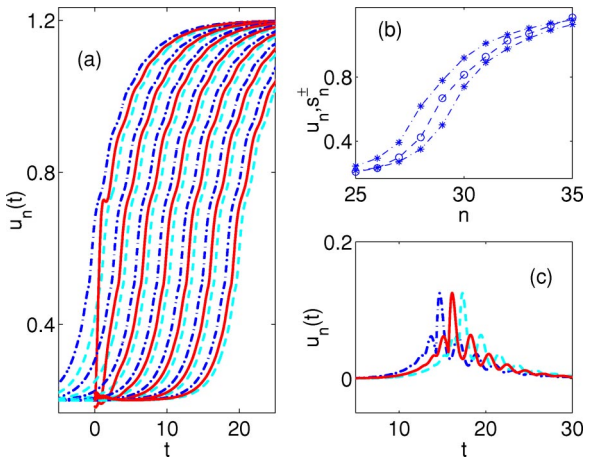

FIG. 4. (Color online) For $D=4$, $\gamma=2.2$, and $F=0.2$: (a) Compared time evolution of $w_n(t+\tau)$ (dot-dashed line), $w_n(t-\tau)$ (dashed line), and $u_n(t)$ (solid line) when $n=0,-1,-2,\ldots$, (b) Compared profiles $u_n(T)$ (circles), $w_n(T\pm\tau)$ (asterisks), (c) Compared time evolution of $w'_n(t\pm\tau)$ (dot-dashed and dashed lines) and $u'_n(t)$ (solid line).

Complex variable methods yield families of explicit wave solutions but give no information on their stability. Numerical tests [10] and physical context [11] suggest the stability of traveling kinks that have monotone leading edges and large enough speeds. Figures 4–6 depict the wave profiles for decreasing γ. We now confirm that these wave fronts are stable. The traveling wave $w_n(t)$ is stable for the dynamics of the chain when the solutions $u_n(t)$ of Eq. (2) remain near $w_n(t)$ for all $t>0$ if the initial states u^0_n, u^1_n are chosen near $w_n(0), w'_n(0)$. Controlling the evolution of $u_n(t)$ is more or less difficult depending on the properties of the Green functions. We distinguish two cases: positive Green functions (large damping) and oscillatory Green functions (small damping).

A. Strong damping

For large damping $\gamma^2\gg 4$, we know that the wave front profiles are monotonically increasing and that the Green

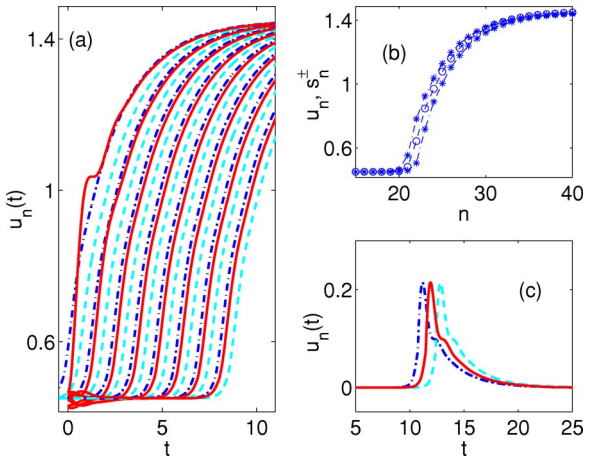

FIG. 5. (Color online) Same as Fig. 4 when $F=0.45$.

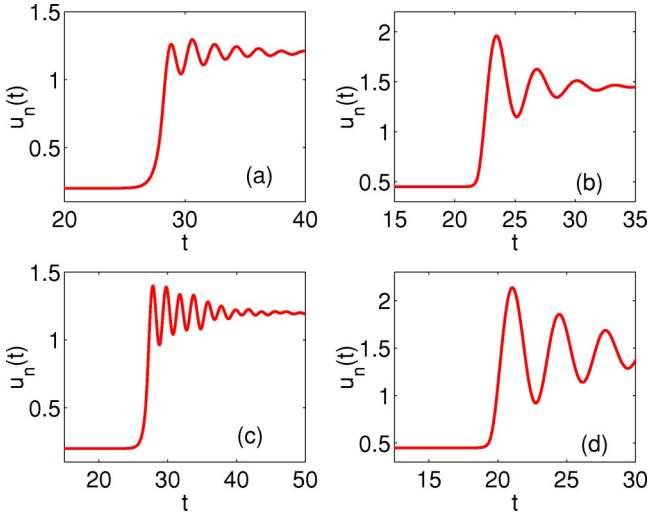

FIG. 6. (Color online) Trajectories $u_n(t)$ when $D=4$. (a) $\gamma=0.2$, $F=0.2$, (b) $\gamma=0.2$, $F=0.45$, (c) $\gamma=0.1$, $F=0.2$, (d) $\gamma=0.1$, $F=0.45$.

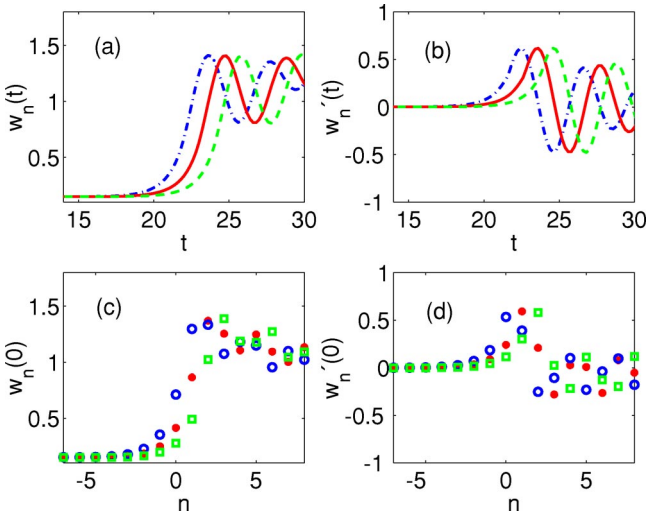

FIG. 7. (Color online) (a) Trajectories $w_{n-1}(t)$ (dash-dotted), $w_n(t)$ (solid), $w_{n+1}(t)$ (dashed); (b) same for $w'_{n-1}(t)$, $w'_n(t)$, $w_{n+1}(t)$; (c) initial configurations for $w_n(\tau)$ (circles), $w_n(0)$ (asterisks), $w_n(-\tau)$ (squares), the vertical line defines n_0; (d) same for $w'_n(\tau)$, $w'_n(0)$, $w'_n(-\tau)$, the vertical lines define n_1.

functions are positive and decay exponentially in time (cf. Appendix B). The main result of this section is the following stability theorem, whose proof can be found in Appendix C:

Theorem. Let us select the wave front profile so that $w_n(t)=w(n-ct-\frac{1}{2})$, with $c<0$, and $F>0$. If we choose the initial states for Eq. (2), u_n^1 and u_n^0, in the set:

$$w_n(-\tau)<u_n^0<w_n(\tau), \quad 0<\tau\ll\frac{1}{2|c|}, \tag{22}$$

$$|w_n'(-\tau)-u_n^1|\ll u_n^0-w_n(-\tau),$$

$$|w_n'(\tau)-u_n^1|\ll w_n(\tau)-u_n^0, \tag{23}$$

then

$$w_n(t-\tau)<u_n(t)<w_n(t+\tau) \tag{24}$$

for all n and $t>0$.

In other words, if the initial oscillator configuration is sandwiched between two wave front profiles with different phase shifts, $w_n(-\tau)$ and $w_n(\tau)$ (with a sufficiently small τ), then the oscillator chain remains trapped between the two shifted profiles $w_n(t-\tau)$ and $w_n(t-\tau)$ forever, provided $|u_n^1-w_n'(0)|$ is sufficiently small. This implies the dynamical stability of the wave. The more involved argument explained in Sec. III B for conservative dynamics can be used to prove that the wave fronts are also asymptotically stable.

Furthermore, the basin of attraction of a particular traveling wave is larger than Eqs. (22) and (23), as shown in Figs. 4 and 5 for $F>F_{cs}(D)$. The initial oscillator configuration in this figure is a step function, $u_n^0=F$ for $n\leqslant 0$ and $u_n^0=1+F$ for $n\geqslant 1$, with a superimposed small random disturbance. The initial velocity profile fluctuates randomly about zero with a small amplitude. After an initial transient, the trajectories get trapped between advanced wave fronts $w_n(t+\tau)$ and delayed wave fronts $w_n(t-\tau)$. Moreover, they converge to a shifted wave front $w_n(t+\alpha)$ as $t\to\infty$.

B. Conservative dynamics

For small damping $\gamma^2\ll 4$, we know that the kink profiles develop oscillations in the trailing edge (see Fig. 6) and that the Green functions oscillate and change sign (cf. Appendix B). However, $G_{nk}^0(t)$ and $G_{nk}^1(t)$ are positive for $0\leqslant t\leqslant T^*=T(\gamma,D)$. This critical time T^* plays a key role for the stable propagation of waves. We will show in this section that kinks are stable provided $|c|>1/T^*$. Our argument does not say anything about the stability of kinks with lesser speeds. Moreover, $T^*\to 0$ and our lower bound on the wave front velocity tends to infinity, in the continuum limit.

We show in Appendix B that a rough estimate for T^* is provided by $2\pi/\sqrt{4(1+4D)-\gamma^2}$. For $\gamma=0$ and $D=4$, as chosen in our Figs. 6 and 7, $T^*>1$. Then, kinks with $|c|>1$ are stable. In Refs. [11,10], stability was conjectured for speeds larger than the last minimum of $F(c)$, which is attained at $c_{cd}\sim 0.74$.

For small or zero damping we cannot use the previous comparison arguments because the trailing edge of the traveling wave front oscillates and monotonicity does not hold there. If we look at the traveling wave front profiles, it becomes clear that we should compare the monotone leading edges of the fronts. Figure 7(a) and 7(b) depict the trajectories $w_n(t)$ and their time derivatives $w_n'(t)$ for a particular traveling wave front. We observe that $w_{n-1}(t)<w_n(t)<w_{n+1}(t)$ and $w'_{n-1}(t)<w'_n(t)<w'_{n+1}(t)$ up to a certain time. Figure 7(c) shows the initial configurations for $w_n(0)$ and the shifted waves $w_n(-\tau)$, $w_n(\tau)$. $w_n(0)$ is sandwiched between $w_n(-\tau)$ and $w_n(\tau)$ up to a point n_0. Figure 7(d) depicts the initial velocity profiles $w_n'(0)$, $w_n'(-\tau)$ and $w_n'(\tau)$. $w_n'(0)$ is sandwiched between $w_n'(-\tau)$, and $w_n'(\tau)$ up to a point n_1. n_0 and n_1 mark the onset of the oscillatory tails. In general, $0\leqslant n_0\leqslant n_1$. As the wave advances, the ranges of n for which $w_n(t-\tau)<w_n(t)=w(n-ct-\frac{1}{2})<w_n(t+\tau)$ change with t.

The main result of this section is the following stability theorem, whose proof can be found in Appendix D:

Theorem. Let us select the wave front profile so that $w_n(t)=w(n-ct-\frac{1}{2})$, with $c<0$ and $F>0$. Let T^* be the maximum time up to which the Green functions $G^0_{nk}(t)$ and $G^1_{nk}(t)$ remain positive. We assume that the speed $|c|>1/T^*$ and choose the initial states for Eq. (2), u^1_n and u^0_n, in the set

$$w_n(-\tau)<u^0_n<w_n(\tau), \quad n\leqslant n_0, \quad 0<\tau\ll\frac{1}{2|c|}, \tag{25}$$

$$w'_n(-\tau)<u^1_n<w'_n(\tau), \quad n\leqslant n_1,$$

$$\sum_n |u^0_n-w_n(0)|<\epsilon, \quad \sum_n |u^1_n-w'_n(0)|<\epsilon \tag{26}$$

for $\epsilon>0$ small and $\tau<\epsilon$. Then, we can find an increasing sequence of times t_k, $k=0,1,\ldots,$ with $t_{-1}=0$, such that:

$$w_n(t-\tau)<u_n(t)<w_n(t+\tau), \quad n\leqslant n_0-k,$$

$$w'_n(t-\tau)<u'_n(t)<w'_n(t+\tau), \quad n\leqslant n_1-k \tag{27}$$

for $t_{k-1}\leqslant t<t_k$. Furthermore, for $t>0$ and any n, we have

$$|u_n(t)-w_n(t)|\leqslant\sum_k |G^1_{nk}(t)||u^0_k-w_k(0)| + \sum_k |G^0_{n0}(t)||u^1_k-w'_k(0)|+C(t), \tag{28}$$

$$C(t)=\sum_{k\leqslant 0,t\geqslant T_k-\tau}\int_{T_k-\tau}^{\min(T_k+\tau,t)} G^0_{nk}(t-z)dz,$$

in which $T_k=k/|c|+1/2|c|$. Thus, the traveling wave front is stable when $\gamma=0$ or asymptotically stable when $\gamma>0$.

Let us clarify the meaning of Eq. (28). For $\gamma>0$, the sums $\Sigma_k|G^1_{nk}(t)|$, $\Sigma_k|G^0_{nk}(t)|$ decay exponentially with time. For small τ, the function $|C(t)|\sim 2\tau\Sigma_{k\leqslant 0,t\geqslant T_k-\tau}|G^0_{nk}(t-T_k)|$. This sum is finite and decays with time. This explains our asymptotical stability claim. When $\gamma=0$, the sums $\Sigma_k|G^1_{nk}(t)||u^0_k-w_k(0)|$, $\Sigma_k|G^0_{nk}(t)||u^0_k-w_k(0)|$ are bounded by a constant time $\max_k|u^0_k-w_k(0)|+\max_k|u^0_k-w_k(0)|$. The function $|C(t)|$ is bounded by a constant time τ and is made small by choosing τ small. This explains our stability claim in the conservative case.

The inequalities (27) tell us that the leading edge of the propagating kink is sandwiched between the leading edges of the shifted traveling wave fronts $w_n(t+\tau)$ and $w_n(t-\tau)$. As the kink $u_n(t)$ advances, the times t_k at which $u_{-k}(t)-\frac{1}{2}$ changes sign are bounded by the times at which the advanced and delayed wave fronts cross $\frac{1}{2}$: $T_k-\tau\leqslant t_k\leqslant T_k+\tau$. This fact is the key for obtaining the stability bound (28).

IV. COEXISTENCE

The results in Sec. III B indicate that stable static and traveling kinks may coexist. The only restriction on the traveling kinks is the monotonicity of the leading edge and a low bound on the speed. These conditions are satisfied by traveling wave fronts for a range of forces in which static wave fronts also exist. We show in this section how oscillating Green functions may force initial kinklike configurations (which would be pinned for large damping) to evolve into a traveling wave front provided the damping is small enough.

We fix $F<F_{cs}$ and select the static kink s_n constructed in Sec. II for Eq. (2) with $s_0<\frac{1}{2}<s_1$. Let the initial condition for Eq. (2) be a piecewise constant profile: $u^0_n=F$ for $n\leqslant 0$, $u^0_n=1+F$ for $n\geqslant 1$ and $u^1_n=0$. Let T^* the maximum time up to which G^0_{nk} and G^1_{nk} remain positive.

As long as $u_n(t)-\frac{1}{2}$ does not change sign for any n, $u_n(t)$ is given by formula (7) in Sec. II. We have $\Sigma_k G^0_{nk}(t)u^1_k\geqslant 0$ for $t\leqslant T^*$. Initially, $G^1_{nk}(t)$ is concentrated at $k=n$ and the sign of $\Sigma_k G^1_{nk}(t)(u^0_k-s_k)$ is decided by the sign of $u^0_n-s_n$. If $u^0_n>s_n$, $u_n(t)\geqslant s_n$. In our case, this is true for $n\geqslant 1$. If $u^0_n<s_n$, $u_n(t)$ increases towards s_n as $\Sigma_k G^1_{nk}(t)(u^0_k-s_k)$ decays. By our choice of the initial state, $u_0(t)$ grows faster than the other components $u_n(t)$, $n<0$.

Now there are two possibilities depending on the value of the damping coefficients. For large damping, $G^1_{nk}(t)$ is positive for all times and G^0_{nk} decays fast. Then $u_0(t)$ cannot surpass s_0. These initial data are pinned for large damping.

For small values of the damping, $G^1_{nk}(t)$ changes sign. Then $u_0(t)$ given by Eq. (7) may surpass s_0 and $\frac{1}{2}$ since the term $\Sigma_k G^1_{nk}(t)(u^0_k-s_k)$ becomes positive for $t\geqslant T^*$. This process can be iterated to get a stably propagating wave, see Fig. 1. A prediction for the speed is found in this way: it is the reciprocal of the time that $s_0+G^1_{00}(t)(F-s_0)$ needs to reach $\frac{1}{2}$.

V. MORE GENERAL POTENTIALS

We have focused our study on periodic piecewise parabolic potentials $V(u)=u^2/2$, $|u|<\frac{1}{2}$. For these potentials, families of static and traveling wave fronts can be constructed analytically. Schmidt [17] and later authors [18,19] found exact monotone wave fronts of conservative systems by constructing models with nonlinearities such that the desired wave fronts were solutions of the models. For damped Frenkel-Kontorova or quartic double-well potentials, stably propagating wave fronts have been found numerically [10]. Numerical studies of kink propagation in the conservative Frenkel-Kontorova model were carried out in Ref. [14].

The stability of propagating kinks in these models can be studied adapting the methods developed in this paper, but the analysis is technically more complicated [16]. For instance, taking $V(u)=u^2/2$ for $|u|<\frac{1}{2}$, $\frac{1}{4}-(u-1)^2/2$ for $|u-1|<\frac{1}{2}$ we get a *continuous* piecewise linear source

$$g(s)=\begin{cases} s, & s<\dfrac{1}{2} \\ -s+\dfrac{1}{2}, & \dfrac{1}{2}<s<\dfrac{3}{2} \\ s-1, & s\geqslant 3/2. \end{cases}$$

The arguments in Secs. III A and III B can be adapted by including new terms $\int_0^t \Sigma 1/2<u_k<3/2 G_{nk}^0(t-z)[2u_k(z)-\frac{1}{2}]dz$ in the integral expressions (C1) and (C2) and using that the function $h(s)=2s-1/2$ is increasing in $1/2<s<3/2$. Similarly, for a Frenkel-Kontorova potential, we write $g(s)=-as+[\sin(s)+as]$, $a>0$. Then, we find the integral expression (A12) with a nonlinear source $f_k=-\sin(u_k)+au_k+F$, using the Green functions for the linear operator $u_n''+\gamma u_n'-D(u_{n+1}-2u_n+u_{n-1})+au_n$. The parameter a is chosen to ensure adequate monotonicity properties for $h(s)=-\sin(s)+as$ [16].

VI. CONCLUSIONS

We have developed a nonlinear stability theory for wave fronts in conservative and damped Frenkel-Kontorova models with piecewise linear sources based on integral formulations. Our results provide an analytical basis for the distinction between static and dynamic Peierls stresses, which arise as thresholds for the existence of stable static and traveling wave fronts. With little or zero damping, stable propagation of fronts is possible when their speeds surpass a critical value. The corresponding wave front profiles have a monotone leading edge, and, possibly, an oscillatory wake. Wave fronts can be oscillatory and yet stable. Whether slow wave fronts showing oscillations in the leading and trailing edges are stable remains an open question [10]. It is remarkable that high order quasicontinuum approximations such as those by Rosenau [20] or by Boussinesq [21] have wave solutions comparable to the fast waves of the discrete conservative model [12].

Together with the stability theory we have presented an algorithm for the numerical computation of the dynamics of kinks. Our scheme has good stability properties and avoids distortions originated by artificial boundary conditions and time discretization.

ACKNOWLEDGMENTS

This work was supported by the Spanish MCyT through Grant No. BFM2002-04127-C02, and by the European Union under Grant No. HPRN-CT-2002-00282. The author thanks Professor L.L. Bonilla for a careful reading of the paper.

APPENDIX A: GREEN FUNCTIONS

We want to find an integral representation of the solution of the problem

$$u_n''+\gamma u_n'=D(u_{n+1}-2u_n+u_{n-1})-u_n+f_n, \qquad \text{(A1)}$$

$$u_n(0)=u_n^0, \quad u_n'(0)=u_n^1 \qquad \text{(A2)}$$

with $\gamma\geqslant 0, D>0$. Firstly, we get rid of the difference operator by using the generating functions $p(\theta,t)$, $f(\theta,t)$:

$$p(\theta,t)=\sum_n u_n(t)e^{-in\theta}, \quad f(\theta,t)=\sum_n f_n(t)e^{-in\theta}. \qquad \text{(A3)}$$

Differentiating p with respect to t and using Eq. (A1), we see that p solves the ordinary differential equation

$$p''(\theta,t)+\gamma p'(\theta,t)+\omega(\theta)^2 p(\theta,t)=f(\theta,t), \qquad \text{(A4)}$$

where $\omega(\theta)^2=1+4D\sin^2(\theta/2)$ and the obvious initial conditions for $p(\theta,t)$ follow from those for $u_n(t)$.

The solution p depends on the roots of the polynomial $r^2+\gamma r+\omega(\theta)^2=0$. When $\gamma^2/4>\omega^2(\theta)$,

$$\begin{aligned} p(\theta,t)=&p(\theta,0)\frac{e^{r_-(\theta)t}r_+(\theta)-e^{r_+(\theta)t}r_-(\theta)}{r_+(\theta)-r_-(\theta)} \\ &+p'(\theta,0)\frac{e^{r_+(\theta)t}-e^{r_-(\theta)t}}{r_+(\theta)-r_-(\theta)} \\ &+\int_0^t \frac{e^{r_+(\theta)(t-s)}-e^{r_-(\theta)(t-s)}}{r_+(\theta)-r_-(\theta)}f(\theta,s)ds \end{aligned} \qquad \text{(A5)}$$

with $r_\pm(\theta)=(-\gamma\pm\sqrt{\alpha(\theta)})/2<0$ and $\alpha(\theta)=\gamma^2-4\omega(\theta)^2$. When $\gamma^2/4<\omega^2(\theta)$, the roots are complex:

$$\begin{aligned} p(\theta,t)=&p(\theta,0)e^{(-\gamma/2)t}\left[\cos[I(\theta)t]+\frac{\gamma\sin[I(\theta)t]}{2I(\theta)}\right] \\ &+p'(\theta,0)e^{(-\gamma/2)t}\frac{\sin[I(\theta)t]}{I(\theta)} \\ &+\int_0^t e^{(-\gamma/2)(t-s)}\frac{\sin[I(\theta)(t-s)]}{I(\theta)}f(\theta,s)ds, \end{aligned} \qquad \text{(A6)}$$

where $I(\theta)=\sqrt{-\alpha(\theta)}/2$. When $\gamma^2/4=\omega^2(\theta)$,

$$\begin{aligned} p(\theta,t)=&p(\theta,0)e^{(-\gamma/2)t}\left(1+\frac{\gamma}{2}t\right)+p'(\theta,0)e^{(-\gamma/2)t}t \\ &+\int_0^t (t-s)e^{(-\gamma/2)(t-s)}f(\theta,s)ds. \end{aligned} \qquad \text{(A7)}$$

The solution $u_n(t)$ of Eq. (A1) is recovered from the definition (A3):

$$u_n(t)=\int_{-\pi}^{\pi}\frac{d\theta}{2\pi}e^{in\theta}p(\theta,t). \qquad \text{(A8)}$$

Here, $p(\theta,t)$ is defined by Eq. (A5) when $\theta\in I_1$,

$$I_1=\left\{\theta\in[-\pi,\pi]\,\middle|\,\frac{\gamma^2}{4}>\omega^2(\theta)\right\}, \qquad \text{(A9)}$$

by Eq. (A6) when $\theta\in I_2$,

$$I_2=\left\{\theta\in[-\pi,\pi]\,\middle|\,\frac{\gamma^2}{4}<\omega^2(\theta)\right\}, \qquad \text{(A10)}$$

and by Eq. (A7) when $\theta\in I_3$,

$$P=\left\{\theta\in[-\pi,\pi]\,\middle|\,\frac{\gamma^2}{4}=\omega^2(\theta)\right\}. \qquad \text{(A11)}$$

Notice that $I_1=P=\varnothing$ if $\gamma^2<4$ and $I_2=P=\varnothing$ if $\gamma^2>4(1+4D)$. $P\neq\varnothing$ only if $4(1+4D)<\gamma^2<4$ and it then consists of two points.

Formula (A8) can be rewritten as

$$u_n(t)=\sum_k\,[G^0_{nk}(t)u'_k(0)+G^1_{nk}(t)u_k(0)] + \int_0^t \sum_k\, G^0_{nk}(t-s)f_k(s)ds, \tag{A12}$$

where

$$G^0_{nk}(t)=\int_{-\pi}^{\pi}\frac{d\theta}{2\pi}\,e^{i(n-k)\theta}g^0(\theta,t),$$

$$G^1_{nk}(t)=\int_{-\pi}^{\pi}\frac{d\theta}{2\pi}\,e^{i(n-k)\theta}g^1(\theta,t) \tag{A13}$$

with

$$g^0(\theta,t)=\begin{cases}\dfrac{e^{r_+(\theta)t}-e^{r_-(\theta)t}}{r_+(\theta)-r_-(\theta)}, & \theta\in I_1\\ e^{(-\gamma/2)t}t, & \theta\in P\\ e^{(-\gamma/2)t}\dfrac{\sin[I(\theta)(t)]}{I(\theta)}, & \theta\in I_2,\end{cases} \tag{A14}$$

$$g^1(\theta,t)=\begin{cases}\dfrac{e^{r_-(\theta)t}r_+(\theta)-e^{r_+(\theta)t}r_-(\theta)}{r_+(\theta)-r_-(\theta)}, & \theta\in I_1\\ e^{(-\gamma/2)t}\left(1+\dfrac{\gamma}{2}t\right), & \theta\in P\\ e^{(-\gamma/2)t}\left[\cos[I(\theta)t]+\dfrac{\gamma\sin[I(\theta)t]}{2I(\theta)}\right], & \theta\in I_2.\end{cases} \tag{A15}$$

For conservative chains, $\gamma=0$, $G^1_{nk}=dG^0_{nk}/dt$, and

$$G^0_{nk}(t)=\int_{-\pi}^{\pi}\frac{d\theta}{2\pi}\,\frac{e^{i(n-k)\theta}}{\omega(\theta)}\sin[\omega(\theta)t]. \tag{A16}$$

Green functions for Hamiltonian chains were studied in Ref. [22] and earlier in Ref. [23]. For overdamped chains, they were computed in Ref. [13].

APPENDIX B: PROPERTIES OF THE GREEN FUNCTIONS

The Green functions for Eq. (A1) and (A2) have three relevant properties: they decay in time, they decay as $|n-k|\to\infty$, and are positive for some time. The property of spatial decay follows from integration by parts in Eq. (A13):

$$G^0_{nk}(t)=\frac{(-1)^l}{i^l(n-k)^l}\int_{-\pi}^{\pi}\frac{d\theta}{2\pi}\,e^{i(n-k)\theta}\frac{\partial^l g^0(\theta,t)}{\partial\theta^l},$$

$$G^1_{nk}(t)=\frac{(-1)^l}{i^l(n-k)^l}\int_{-\pi}^{\pi}\frac{d\theta}{2\pi}\,e^{i(n-k)\theta}\frac{\partial^l g^1(\theta,t)}{\partial\theta^l} \tag{B1}$$

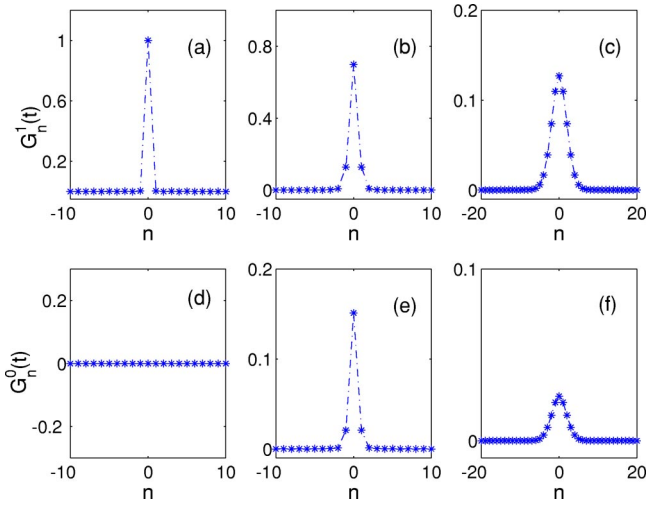

FIG. 8. (Color online) Time evolution of the Green functions for $D=4$ and $\gamma=10$: (a) $t=0$, (b) $t=0.5$, (c) $t=5$; (d) $t=0$, (e) $t=0.5$, (f) $t=5$.

when $n\neq k$. An immediate consequence is that $\Sigma_k|G^0_{nk}(t)|^p$ and $\Sigma_k|G^1_{nk}(t)|^p$ are finite for any $p\geqslant 1$. Therefore, we may obtain decay results as $|n|\to\infty$ for the solutions $u_n(t)$ of Eqs. (A1) and (A2) given by Eq. (A12) decay when the data u^0_n, u^1_n, $f_n(t)$ decay. Figures 8 and 9 illustrate the spatial decay of $G^0_n(t)=G^0_{n0}(t)$ and $G^1_n(t)=G^1_{n0}(t)$. Notice that, initially, both are concentrated about $n=0$.

Time decay and positivity depend on the strength of the damping. Let us start by the *strongly damped case:* $\gamma^2>4(1+4D)$. The Green functions are given by Eqs. (A13)–(A15) with $I_2=P=\varnothing$.

(1) $G^0_{nk}(t)$ *and* $G^1_{nk}(t)$ *are positive.* The roots $r_\pm(\theta)$ being even with respect to θ, both $G^0_{nk}(t)$ and $G^1_{nk}(t)$ are real and $e^{i(n-k)\theta}$ can be replaced by $\cos[(n-k)\theta]$. The kernels $g_0(\theta,t)=(e^{r_+(\theta)t}-e^{r_-(\theta)t})/[r_+(\theta)-r_-(\theta)]$ and $g_1(\theta,t)$

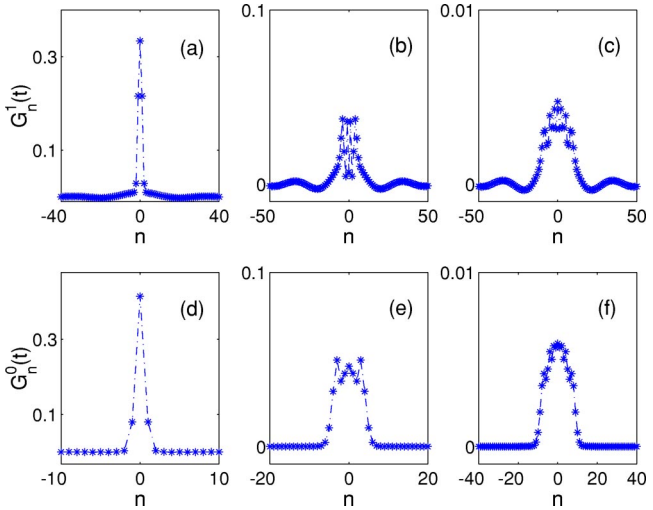

FIG. 9. (Color online) Time evolution of the Green functions for $D=4$ and $\gamma=2.2$: (a) and (d) $t=0.5$, (b) and (e) $t=2.5$, (c) and (f) $t=5$.

$=(e^{r_-(\theta)t}r_+(\theta)-e^{r_+(\theta)t}r_-(\theta))/[r_+(\theta)-r_-(\theta)]$ are even, positive, reach their maximum values at $\theta=0$, and decay as θ increases to π. The dominant contribution to the integrals (A13) comes from a neighborhood centered at $\theta=0$, where the oscillatory multiplier $\cos[(n-k)\theta]$ is positive. Thus, both $G^0_{nk}(t)$ and $G^1_{nk}(t)$ are positive. Figure 8 illustrates their evolution as time grows. Notice the resemblance with the time evolution of heat kernels.

(2) $G^0_{nk}(t)$ and $G^1_{nk}(t)$ are bounded uniformly in n,k by decaying exponentials in time:

$$|G^0_{nk}(t)| \leqslant \frac{e^{r_+(0)t}-e^{r_-(\pi)t}}{\sqrt{\gamma^2-4(1+4D)}},$$

$$|G^1_{nk}(t)| \leqslant \frac{e^{r_-(\pi)t}r_+(\pi)-e^{r_+(0)t}r_-(0)}{\sqrt{\gamma^2-4(1+4D)}}. \qquad \text{(B2)}$$

We come now to *intermediate damping* $4<\gamma^2<4(1+4D)$. In this case both I_1 and I_2 are nonempty. The piecewise defined kernels g_0 and g_1 are still even, take the largest values near zero (in I_1) and the smallest near π (in I_2). The dominant contribution to $G^0_{nk}(t)$ and $G^1_{nk}(t)$ comes thus from I_1 and is positive. This is helped by the fact that the contribution coming from I_2 is initially positive and the factor $e^{-(\gamma/2)t}$ in the oscillatory region I_2 decays faster than the factor $e^{r_+(\theta)t}$ in the positive region I_1. Therefore, $G^0_{nk}(t)$ and $G^1_{nk}(t)$ are essentially positive in this intermediate regime, see Fig. 9. This means that their large components are positive, despite the appearance of some negligible negative components. They can be roughly bounded by

$$|G^0_{nk}(t)| \leqslant C_0 e^{r_+(0)t}, \quad |G^1_{nk}(t)| \leqslant C_1 e^{r_+(0)t}. \qquad \text{(B3)}$$

We address finally the *weakly damped problems with* $\gamma^2<4$. In this case, $I_1=P=\varnothing$. $G^0_{nk}(t)$ and $G^1_{nk}(t)$ are no longer globally positive. However, the kernels $g_0(\theta,t)$ and $g_1(\theta,t)$ are positive for $|t|<2\pi/\sqrt{4(1+4D)-\gamma^2}=2T$ and $|t|<\pi/\sqrt{4(1+4D)-\gamma^2}=T$, respectively. That means that $G^0_{nk}(t)>0$ and $G^1_{nk}(t)>0$ for t in those intervals. They remain essentially positive in a larger interval. The kernels $g_0(\theta,t)$ and $g_1(\theta,t)$ become negative for θ near π and remain positive for small θ. This is enough for the relevant values of $G^1_{nk}(t)$ to remain positive up to a critical time T^*, often larger than T. We can get uniform bounds in time:

$$|G^0_{nk}(t)| \leqslant \frac{2}{\sqrt{4-\gamma^2}}\, e^{-(\gamma/2)t},$$

$$|G^1_{nk}(t)| \leqslant \left(1+\frac{\gamma}{\sqrt{4-\gamma^2}}\right) e^{-(\gamma/2)t}. \qquad \text{(B4)}$$

The same positivity properties and bounds are shared by the Green functions in the *conservative case* $\gamma=0$. Figures 10 and 11 illustrate the time evolution of the Green functions. A detailed study of the decay properties with respect to n and t for conservative problems can be found in Ref. [22].

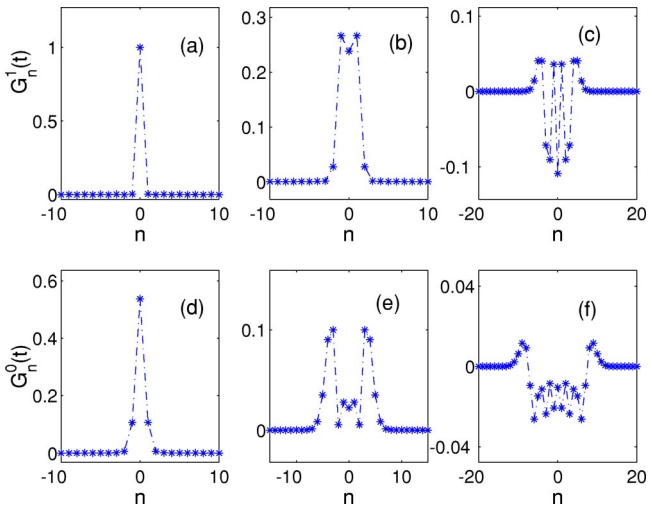

FIG. 10. (Color online) Time evolution of the Green functions for $D=4$ and $\gamma=1$: (a) $t=0$, (b) $t=0.5$, (c) $t=2.5$; (d) $t=0.5$, (e) $t=2.5$, (f) $t=5$.

APPENDIX C: STABILITY OF TRAVELING WAVE FRONTS FOR STRONG DAMPING

We now prove the stability theorem of Sec. III A for strong damping. The key idea of the proof is suggested by formula (5). When we solve Eq. (2) starting from different steplike initial states, we observe three types of terms in Eq. (5). The second and the third are increasing functions of the steplike configurations. The fourth term does not depend on the initial configuration. The first one can be made small by choosing a small velocity profile. Our proof proceeds in two steps. First, we establish a few properties of the traveling wave fronts. Second, we prove the stability bound (24).

Step 1: Basic properties of the traveling waves. For every k, we know that $w_k'(t)>0$. Thus, each $w_k(t)$ crosses $\frac{1}{2}$ at a definite time t_k. Recall that we have selected the unique wave profile $w(x)$ satisfying $w(0)=\frac{1}{2}$. Therefore, $w_{-k}(t)$

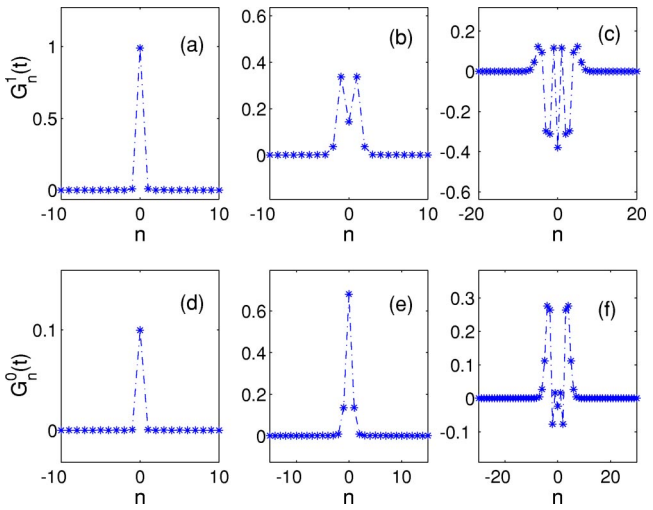

FIG. 11. (Color online) Time evolution of the Green functions for $D=4$ and $\gamma=0$: (a) and (d) $t=0.05$, (b) and (e) $t=0.5$, (c) and (f) $t=2.5$.

$-\frac{1}{2}$ changes sign at time $T_k=k/|c|+1/2|c|>0$, $k=0,1,2,\ldots$. For the shifted waves $w_k(t+\tau)$ and $w_k(t-\tau)$ the changes of sign take place at the shifted times $T_k^+=T_k-\tau$ and $T_k^-=T_k+\tau$.

The waves $w_n(t\pm\tau)$ solve the integral equation (5) with initial data $w_n(\pm\tau)$ and $w_n'(\pm\tau)$. Using the times $T_k^\pm$, we can rewrite formula (5) in a more explicit form:

$$w_n(t\pm\tau)=\sum_k\,[G_{nk}^0(t)w_k'(\pm\tau)+G_{nk}^1w_k(\pm\tau)]+F\int_0^t\sum_k\,G_{nk}^0(t-z)dz+\int_0^t\sum_{k>0}G_{nk}^0(t-z)dz+\sum_{k\leqslant 0}\int_{T_k^\pm}^{\mathrm{Max}(t,T_k^\pm)}G_{nk}^0(t-z)dz. \tag{C1}$$

A term $\int_{T_k^\pm}^t G_{n,k}^0(t-z)dz$ is added whenever a factor $w_k(z\pm\tau)-\frac{1}{2}$ changes sign.

Step 2: Comparing $u_n(t)$ and $w_n(t\pm\tau)$. During the initial stage of the evolution of the chain $u_0(t)<\frac{1}{2}<u_1(t)$ and formula (5) reads

$$u_n(t)=\sum_k\,[G_{nk}^0(t)u_k^1+G_{nk}^1(t)u_k^0]+\int_0^t\sum_{k>0}G_{nk}^0(t-z)dz+F\int_0^t\sum_k\,G_{nk}^0(t-z)dz. \tag{C2}$$

By Eq. (22) and the positivity of $G_{nk}^1(t)$,

$$\sum_k\,G_{nk}^1(t)w_k(-\tau)<\sum_k\,G_{nk}^1(t)u_k^0<\sum_k\,G_{nk}^1(t)w_k(\tau). \tag{C3}$$

By Eq. (23),

$$\sum_k\,G_{nk}^1(t)[w_k(\tau)-u_k^0]+G_{nk}^0(t)[w_k'(\tau)-u_k^1]>0,$$

$$\sum_k\,G_{nk}^1(t)[u_k^0-w_k(-\tau)]+G_{nk}^0(t)[u_k^1-w_k'(-\tau)]>0. \tag{C4}$$

Therefore, Eqs. (C1)–(C4) imply

$$w_n(t-\tau)<u_n(t)<w_n(t+\tau), \tag{C5}$$

for all n and $t\leqslant T_0^+$. Recall that $T_0^+\leqslant T_0^-$ by definition. Afterwards, $w_0(t+\tau)$ has crossed $\frac{1}{2}$ and $\int_{T_0^+}^t G_{n0}^0(t-z)dz>0$ must be added in the expression for $w_n(t+\tau)$. The ordering (C5) still holds. At time T_0^-, $w_0(t-\tau)$ crosses $\frac{1}{2}$. By Eq. (C4), $u_0(t)$ must cross before, at a time t_0.

In this way, we obtain a sequence of times t_k at which $u_{-k}(t)-\frac{1}{2}$, changes sign satisfying $T_k^+<t_k<T_k^-$, $k=0,1,2,\ldots$. Then,

$$u_n(t)=\sum_k\,[G_{nk}^0(t)u_k^1+G_{nk}^1(t)u_k^0]+F\int_0^t\sum_k\,G_{nk}^0(t-z)dz+\int_0^t\sum_{k>0}G_{nk}^0(t-z)dz+\sum_{k\leqslant 0}\int_{t_k}^{\mathrm{Max}(t,t_k)}G_{nk}^0(t-z)dz \tag{C6}$$

and Eq. (C5) holds for all t. Our stability claim is proved.

APPENDIX D: STABILITY OF TRAVELING WAVE FRONTS FOR CONSERVATIVE DYNAMICS

In this section, we prove the stability theorem of Sec. III B for small or zero damping. The notation is the same as in Appendix C and the proof is organized in two steps.

Step 1: Initial stage. We compare $u_n(t)$ given by Eq. (C2) with the shifted waves $w_n(t\pm\tau)$ given by Eq. (C1), whereas $u_n'(t)$ is compared with $w_n'(t\pm\tau)$. The time derivatives are calculated by differentiating Eqs. (C1) and (C2). Notice that $dG_{nk}^0(t)/dt>0$ for small damping when $t\leqslant T^*$. Up to a first critical time T_0^+, $u_k(t)-\frac{1}{2}$ and $w_k(t\pm\tau)-\frac{1}{2}$ keep their sign for all k. Therefore,

$$w_n(t-\tau)<u_n(t)<w_n(t+\tau),\quad n\leqslant n_0,$$

$$w_n'(t-\tau)<u_n'(t)<w_n'(t+\tau),\quad n\leqslant n_1, \tag{D1}$$

for $t\leqslant T_0^+$. Recall that, initially, G_{nk}^1 and G_{nk}^0, together with their derivatives, take on their maximum values for k close to n. This fact and Eqs. (24) and (25) imply

$$w_n(t-\tau)<u_n(t)<w_n(t+\tau),\quad n\leqslant n_0-1,$$

$$w_n'(t-\tau)<u_n'(t)<w_n'(t+\tau),\quad n\leqslant n_1-1, \tag{D2}$$

for $T_0^+\leqslant t\leqslant T_1^+$, choosing $\tau<T^*-T_0$. This means that $u_0(t)-\frac{1}{2}$ changes sign at a time t_0 such that $T_0^+<t_0<T_0^-<T_1^+$. We then obtain formula (C6) for $u_n(t)$ restricted to $t\leqslant T_1^+$. By substracting Eq. (C1) from Eq. (C6), we find

$$\sum_n\,|u_n-w_n|(t)\leqslant\sum_n\,|G_{n0}^1(t)|\sum_n\,|u_n-w_n|(0)+\sum_n\,|G_{n0}^0(t)|\sum_n\,|u_n'-w_n'|(0)+C(t), \tag{D3}$$

where

$$C(t)=\begin{cases} 0, & t\leqslant T_0^+ \\ \int_{T_0^+}^{T_0^-} G_{n0}^0(t-z)dz, & t>T_0^+, \end{cases}$$

and

$$\sum_n |u_n'-w_n'|(t)\leqslant \sum_n \left|\frac{dG_{n0}^1}{dt}(t)\right| \sum_n |u_n-w_n|(0) + \sum_n \left|\frac{dG_{n0}^0}{dt}(t)\right| \sum_n |u_n'-w_n'|(0)+R(t), \tag{D4}$$

where

$$R(t)=\begin{cases} 0, & t\leqslant T_0^+ \\ \int_{T_0^+}^{T_0^-} \frac{dG_{n0}^0}{dt}(t-z)dz, & t>T_0^+, \end{cases}$$

for $t\leqslant T_1^+$. Let $S_1=\mathrm{Max}_{[0,\infty)}\Sigma_n|G_{n0}^1(t)|$, $S_2=\mathrm{Max}_{[0,\infty)}\Sigma_n|G_{n0}^0(t)|$, $S_3=\mathrm{Max}_{[0,\infty)}\Sigma_n|(dG_{n0}^1/dt)(t)|$, and $S_4=\mathrm{Max}_{[0,\infty)}\Sigma_n|(dG_{n0}^0/dt)(t)|$. Then, for $t\leqslant T_1^+$,

$$\sum_n |u_n(t)-w_n(t)|\leqslant (S_1+S_2)\varepsilon+2\tau|G_{n0}^0(T_0)|,$$

$$\sum_n |u_n'(t)-w_n'(t)|\leqslant (S_3+S_4)\varepsilon+2\tau\left|\frac{dG_{n0}^0}{dt}(T_0)\right|. \tag{D5}$$

The distances $|u_n(t)-w_n(t)|$, $|u_n'(t)-w_n'(t)|$ remain of order ε. In particular, the oscillatory tail of $u_n(t)$ for $n>n_0$ is contained in the same band that contains $w_n(t)$ for $n>n_0$.

Step 2: Generic stage. We iterate Step 1 starting at times T_l^+, $l=1,2,\ldots$, according to the following induction procedure. For a fixed T_l^+, Eq. (D2) holds for $n<n_0-l$, $n<n_1-l$, $T_{l-1}^+\leqslant t\leqslant T_l^+$, and

$$\sum_n |u_n(t)-w_n(t)|\leqslant (S_1+S_2)\varepsilon+2\tau S,$$

$$\sum_n |u_n'(t)-w_n'(t)|\leqslant (S_3+S_4)\varepsilon+2\tau S \tag{D6}$$

holds for $t\leqslant T_l^+$, with $S=\mathrm{Max}[\Sigma_k|G_{nk}^0(T_k)|,\Sigma_k|(dG_{nk}^0/dt)\times(T_k)|]$. Now, we shall show that these properties also hold for T_{l+1}^+.

For $T_l^+\leqslant t\leqslant T_{l+1}^+$, the evolution of $w_n(t\pm\tau)$ and $u_n(t)$ is given by

$$\begin{aligned} w_n(t\pm\tau)=&\sum_k G_{nk}^0(t-T_l^+)w_k'(T_l^+\pm\tau) \\ &+\sum_k G_{nk}^1(t-T_l^+)w_k(T_l^+\pm\tau) \\ &+F\int_{T_{l-1}^-}^t \sum_k G_{nk}^0(t-z)dz \\ &+\int_{T_l^+}^t \sum_{k>-l} G_{nk}^0(t-z)dz \\ &+\sum_{k\leqslant -l}\int_{T_k^\pm}^{\mathrm{Max}\,(t,T_k^\pm)} G_{nk}^0(t-z)dz, \end{aligned} \tag{D7}$$

$$\begin{aligned} u_n(t)=&\sum_k G_{nk}^0(t-T_l^+)u_k'(T_l^+)+\sum_k G_{nk}^1(t-T_l^+)u_k(T_l^+) \\ &+F\int_{T_l^+}^t \sum_k G_{nk}^0(t-z)dz+\int_{T_l^+}^t \sum_{k>-l} G_{nk}^0(t-z)dz \\ &+\sum_{k\leqslant -l}\int_{T_l^+}^t G_{nk}^0(t-z)H\left[u_k(z)-\frac{1}{2}\right]dz. \end{aligned} \tag{D8}$$

Notice that we have taken as initial data the values of $w_n(t\pm\tau)$ and $u_n(t)$ at time T_l^+. In this way, formulas (D7) and (D8) only involve the values of the Green functions in a short time interval $[0,1/|c|+2\tau]$. Since $1/|c|+2\tau>T^*$, the Green functions are both positive. Recall that for this short time interval G_{nk}^1 and G_{nk}^0, together with their derivatives, take on large values for k close to n. We can then use Eq. (D2) for $n<n_0-l$, $n<n_1-l$ at time T_l^+, Eqs. (D6)–(D8) to obtain Eq. (D2) for $n<n_0-(l+1)$, $n<n_1-(l+1)$, and $T_l^+\leqslant t\leqslant T_{l+1}^+$. This means that $u_{-l}(t)-\frac{1}{2}$ changes sign at a time t_l such that $T_l^+<t_l<T_l^-<T_{l+1}^+$. We then obtain formula (C6) for $u_n(t)$ restricted to $t\leqslant T_{l+1}^+$. Subtracting Eq. (C1) from Eq. (C6) for $t\leqslant T_{l+1}^+$, we find

$$\sum_n |u_n-w_n|(t)\leqslant (S_1+S_2)\varepsilon+2\tau\sum_{k\leqslant l}|G_{nk}^0(T_k)|,$$

$$\sum_n |u_n'-w_n'|(t)\leqslant (S_3+S_4)\varepsilon+2\tau\sum_{k\leqslant l}\left|\frac{dG_{nk}^0}{dt}(T_k)\right|. \tag{D9}$$

This implies Eq. (D6) for $t\leqslant T_{l+1}^+$. We are now ready to repeat the process starting at time T_{l+1}^+.

Step 3: Conclusion. From Step 2 we obtain a sequence of times t_l for $l=1,2,\ldots$, with $T_l^+<t_l<T_l^-$, at which $u_{-l}(t)-\frac{1}{2}$ changes sign. In this way, we keep track of the times t_l at which changes of sign take place and obtain formula (C6) for $u_n(t)$ for all t. Subtracting Eq. (C1) from Eq. (C6) we find the bound (28) on $|u_n-w_n|$.

[1] J. Frenkel and T. Kontorova, Phys. Z. Sowjetunion **13**, 1 (1938) [J. Phys. (USSR) **1**, 137 (1939)]; O.M. Braun and Yu.S. Kivshar, Phys. Rep. **306**, 1 (1998).
[2] F.R.N. Nabarro, *Theory of Crystal Dislocations* (Oxford University Press, Oxford, UK, 1967).
[3] L.I. Slepyan, Sov. Phys. Dokl. **26**, 538 (1981).
[4] P.M. Chaikin and T.C. Lubensky, *Principles of Condensed Matter Physics* (Cambridge University Press, Cambridge, 1995), Chap. 10.
[5] L.L. Bonilla, J. Phys.: Condens. Matter **14**, R341 (2002).
[6] A. Tonnelier, Phys. Rev. E **67**, 036105 (2003); A. Anderson and B. Sleeman, Int. J. Bifurcation Chaos Appl. Sci. Eng. **5**, 63 (1995).
[7] J.P. Keener and J. Sneyd, *Mathematical Physiology* (Springer, New York, 1998), Chap. 9.
[8] R. Hobart, J. Appl. Phys. **36**, 1948 (1965).
[9] E. Gerde and M. Marder, Nature (London) **413**, 285 (2001); D.A. Kessler, *ibid.* **413**, 260 (2001).
[10] A. Carpio and L.L. Bonilla, Phys. Rev. E **67**, 056621 (2003).
[11] W. Atkinson and N. Cabrera, Phys. Rev. **138**, A763 (1965).
[12] O. Kresse and L. Truskinovsky, J. Mech. Phys. Solids **51**, 1305 (2003).
[13] G. Fáth, Physica D **116**, 176 (1998); A. Carpio and L.L. Bonilla, Phys. Rev. Lett. **86**, 6034 (2001).
[14] M. Peyrard and M.D. Kruskal, Physica D **14**, 88 (1984).
[15] A. Carpio, L.L. Bonilla, A. Wacker, and E. Schöll, Phys. Rev. E **61**, 4866 (2000).
[16] A. Carpio (unpublished).
[17] V.H. Schmidt, Phys. Rev. B **20**, 4397 (1979).
[18] P.C. Bressloff and G. Rowlands, Physica D **106**, 255 (1997).
[19] S. Flach, Y. Zolotaryuk, and K. Kladko, Phys. Rev. E **59**, 6105 (1999).
[20] P. Rosenau, Phys. Lett. A **118**, 222 (1986).
[21] M.J. Boussinesq, J. Math. Pures Appl. **17**, 55 (1872).
[22] J. Bafaluy and J.M. Rubi, Physica A **153**, 129 (1988); **153**, 147 (1988).
[23] E. Schrödinger, Ann. Phys. (Leipzig) **44**, 1053 (1914).